ChemPubSoc Europe

DOI: 10.1002/open.201900350

Open Access ChemistryOPEN Full Papers

Special Issue

Halogenation of the *N*-Terminus Tyrosine 10 Promotes Supramolecular Stabilization of the Amyloid-β Sequence 7–12

Daniele Maiolo[+],[a] Andrea Pizzi[+],[a] Alessandro Gori,[b] Lara Gazzera,[a] Nicola Demitri,[c] Alessandro Genoni,[d] Fulvio Baggi,[e] Fabio Moda,[e] Giancarlo Terraneo,*[a, b] Francesca Baldelli Bombelli,[a] Pierangelo Metrangolo,*[a] and Giuseppe Resnati[a]

This paper is dedicated to Prof. Jean-Marie Lehn on his 80th birth anniversary.

Here, we demonstrate that introduction of halogen atoms at the tyrosine 10 phenol ring of the DSGYEV sequence derived from the flexible amyloid-β *N*-terminus, promotes its self-assembly in the solid state. In particular, we report the crystal structures of two halogen-modified sequences, which we found to be stabilized in the solid state by halogen-mediated interactions. The structural study is corroborated by Non-Covalent Interaction (NCI) analysis. Our results prove that selective halogenation of an amino acid enhances the supramolecular organization of otherwise unstructured biologically-relevant sequences. This method may develop as a general strategy for stabilizing highly polymorphic peptide regions.

1. Introduction

Alzheimer's disease (AD) is an oxidative stress associated pathology characterized by the accumulation in the Central Nervous System of misfolded amyloid-beta (Aβ) peptides in the form of oligomers and amyloid fibrils.[1] From a structural point of view, the Aβ peptide comprises two regions with β-strand propensity (residues 16–24 and 31–40), two regions with high PPII-helix propensity (residues 1–4 and 11–15), and two unstructured regions with higher mobility (residues 5–10 and 25–30) connecting the structural elements.[2] While Aβ fibrils and neurofibrillary tangles are well-defined signatures of AD,[3] the precise molecular mechanisms underlying their formation and role on disease progression are not completely understood, yet.[4] In fact, for years these structures were considered the only species leading to AD, but more recently Aβ soluble oligomers were also recognized as key actors in the development of the pathology.[5,6] In particular, it has been demonstrated that the *N*-terminus (*N*-term) moieties of these neurotoxic dysfunctional Aβ oligomers are implicated in the development of the disease.[7]

In this context, it is now emerging clearly that the Aβ *N*-term is often site of amino acidic mutations, protein post translational modifications, and of interaction with other proteins, metal cations, and cellular membranes. For example, it has been observed that genetic variants of Aβ peptides with an amino acidic mutation in position 2 of the *N*-term are characterized by different aggregation kinetics, metal site structure, and metal affinity, and showed opposite effects on the onset and progression of AD.[8–11] Of considerable interest, the oxidative stress-related nitration of the Aβ *N*-term tyrosine Y10, as well as oligomers containing cross-linked Y10, were recently described to modify the assembly of the Aβ peptide, and thus the onset and progression of the disease.[12] Overall, all of these results promoted a considerable interest in the *N*-term region as potential hotspot for new therapeutic targets.[13–15]

In this scenario, a precise structural characterization of the Aβ peptide would significantly help the design and development of specific therapeutics. However, being the *N*-term region characterized by a high degree of flexibility, its high-resolution structural features are not easily obtained by X-Ray Diffraction (XRD) and Solid-State Nuclear Magnetic Resonance

[a] Dr. D. Maiolo,[+] Dr. A. Pizzi,[+] Dr. L. Gazzera, Prof. Dr. G. Terraneo, Prof. Dr. F. Baldelli Bombelli, Prof. Dr. P. Metrangolo, Prof. Dr. G. Resnati
Dept. Chem., Mater., and Chem. Eng. "Giulio Natta"
Politecnico di Milano
Via L. Mancinelli 7, 20131 Milano, Italy
E-mail: giancarlo.terraneo@polimi.it
pierangelo.metrangolo@polimi.it
[b] Dr. A. Gori, Prof. Dr. G. Terraneo
Istituto di Scienze e Tecnologie Chimiche
National Research Council of Italy
Via M. Bianco 9, 20131 Milano, Italy
[c] Dr. N. Demitri
Elettra – Sincrotrone Trieste
S.S. 14 Km 163.5 in Area Science Park
34149 Basovizza – Trieste, Italy
[d] Dr. A. Genoni
Laboratoire de Physique et Chimie Théoriques
Université de Lorraine and CNRS
UMR CNRS 7019, 1 Boulevard Arago, 57078 Metz, France
[e] Dr. F. Baggi, Dr. F. Moda
Fondazione IRCCS Istituto Neurologico "Carlo Besta"
Via G. Celoria 11, 20133 Milan, Italy
[+] These two authors contributed equally.

Supporting information for this article is available on the WWW under https://doi.org/10.1002/open.201900350

Special Issue An invited contribution to a Special Collection dedicated to Functional Supramolecular Systems

(SS NMR) studies. Thus, various protein-engineered scaffolds have been adopted to stabilize the Aβ *N*-term region towards crystallization.[16,17] In this regard, halogenation of phenylalanine, a non-natural peptide modification, has recently been proposed as a new tool in peptide and protein engineering.[18] More relevant to the present study, we proposed it as a strategy for promoting crystallization of a highly fibrillating short peptide sequence derived from human calcitonin.[19a,b] The same modification was also found to exacerbate the self-assembly of another highly fibrillating core sequence derived from Aβ, *i.e.*, KLVFF.[19c,d]

Here, knowing that the Y10 of the Aβ *N*-term may also be a putative target of halogenative stress,[20] we investigated the effect of Y10 halogenation on the self-assembly behavior of a core sequence derived from the Aβ *N*-term, *i.e.*, DSGYEV (Aβ 7–12, Scheme 1). To elucidate the role of Y10 halogenation in the supramolecular organization of DSGYEV in the solid state, single crystals of the brominated and chlorinated derivatives were grown and their structures obtained through synchrotron radiation. Differently, the WT-peptide only formed poorly scattering crystals upon drying. High resolution crystal structures of brominated and chlorinated Aβ 7–12 derivatives, along with computational studies, namely Non-Covalent Interaction (NCI) analysis, confirmed the dramatic effect that the halogenation has on the solid state supramolecular stabilization of this otherwise unstructured and highly flexible motif.

2. Results and Discussion

2.1. Single-Crystal X-Ray Diffraction Studies

To study the effect of halogen atom modification on supramolecular stabilization of the highly fibrillogenic and flexible sequence DSGYEV, we introduced I, Br, and Cl atoms at both *ortho*-positions to the tyrosine phenol group, obtaining its diiodo (DSGY(3,5-I)EV), dibromo (DSGY(3,5-Br)EV), and dichloro (DSGY(3,5-Cl)EV) analogues (Scheme 1). Brominated and chlorinated peptides crystallized from water. The WT-peptide and the iodinated Y10 analogue, unfortunately, did not yield crystals suitable for X-ray diffractions analysis.

DSGY(3,5-Br)EV and DSGY(3,5-Cl)EV crystallized in the $P2_1$ space group and were almost isostructural. Both asymmetric units consisted of two independent peptide molecules in an extended β-strand conformation and different water content (Figure 1 and Table S1). In both the halogenated sequences, the peptide strands interacted in a head-to-tail fashion through an extended network of intermolecular hydrogen bonds (HBs) occurring between the amide moieties of stacked backbones (N···O distance is in the range 2.78–3.16 Å) forming the characteristic supramolecular ring-like structure of antiparallel arrangement (Figure 2a). The distance between hydrogen-bonded peptide strands (Figure 2b) is 4.74 Å for the brominated peptide, and a bit longer (4.78 Å) for the chlorinated one. This structural feature is within the range of typical amyloid structures. The antiparallel arrangement propagated along the *a*-crystallographic axis, giving rise to the classical β-pleated sheet (Figures S2 and S3).

Interestingly, the halogen atoms are involved in various intermolecular contacts that stabilize the overall β-sheet structure (Figure 3). Specifically, a short contact between one Br atom (Br1_24) and an O atom (OE1_15) (see CIFs) of the glutamic acid side chain of an adjacent peptide is observed in the DSGY(3,5-Br)EV sequence (Figure 3, top). Although relatively long, this contact showed the typical directionality of a halogen bond (HaB),[21] the C–Br···O angle being 176° and the Br···O distance 3.36(2) Å. This HaB occurs perpendicular to a hydrogen bond between the same oxygen of the glutamic acid and the hydrogen of a water molecule.[22] Similarly, in DSGY(3,5-Cl)EV a non-covalent interaction involving the Cl atom (Cl1_14) and one O atom (OD_21) of the carboxylic group of the Asp residue of a close-by fragment was present (Figure 3, bottom). Also in this case, the interaction distance between the HaB donor and acceptor is long, being at the limit of the sun of the van der Waals radii (Cl···O distance 3.43(3) Å), however, the C–Cl···O angle is close to linearity (168°), which is a structural feature of a classical HaB. The behavior observed in the two sequences

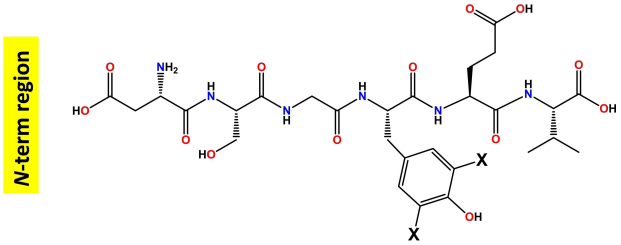

$A\beta_{7\text{-}12}$ DSGY(3,5-X)EV
X = H, Cl, Br, I

Scheme 1. Molecular structures of the studied peptides.

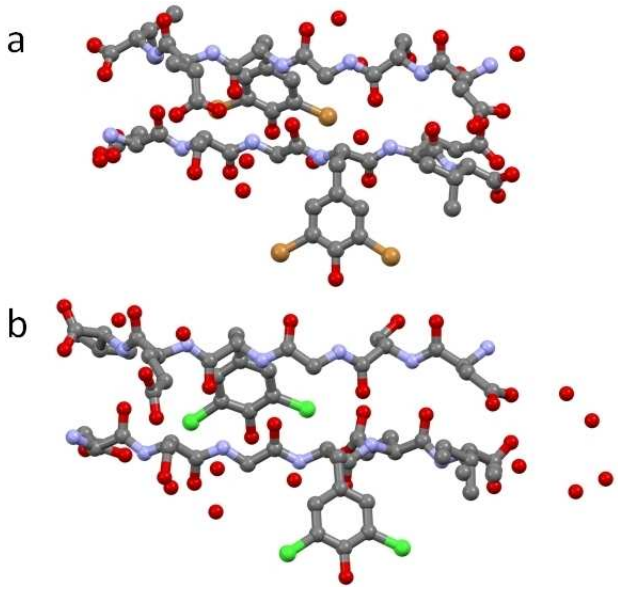

Figure 1. Crystal structures of DSGY(3,5-Br)EV (a) and DSGY(3,5-Cl)EV (b); Asymmetric unit content showing two peptide strands and several water molecules. Colour code: Carbon, grey; Nitrogen, violet; Oxygen, red; Bromine, orange; Chlorine, light green. Hydrogen atoms have been omitted for clarity.

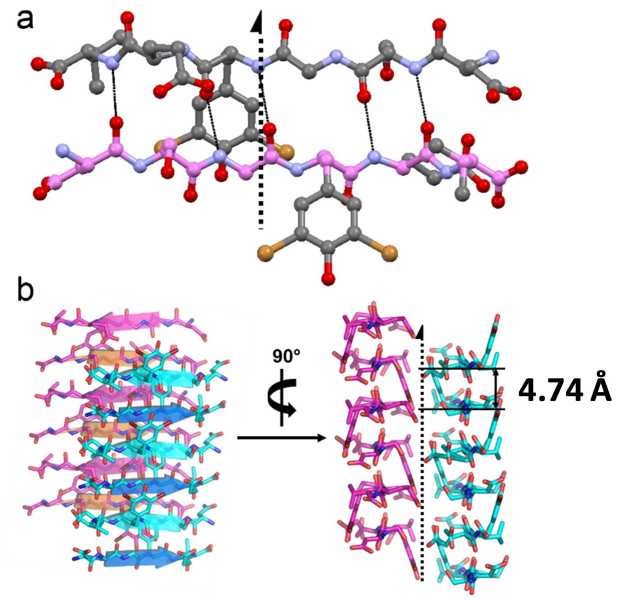

Figure 2. (a) Crystal structure of DSGY(3,5-Br)EV where the peptides form a β-sheet pattern promoted by hydrogen bonds (dashed lines) between the nitrogen and the carbonyl groups of two facing strands. Colour code: C, grey and pink; N, violet; O, red and Br, orange. Hydrogen atoms are omitted for clarity. (b) Orthogonal views of the assemblies of DSGY(3,5-Br)EV. The cross β-spines report the classical structural features of amyloidogenic peptides: Each peptide strand assembles in β-sheet, where the distance between centroid strands is 4.74 Å.

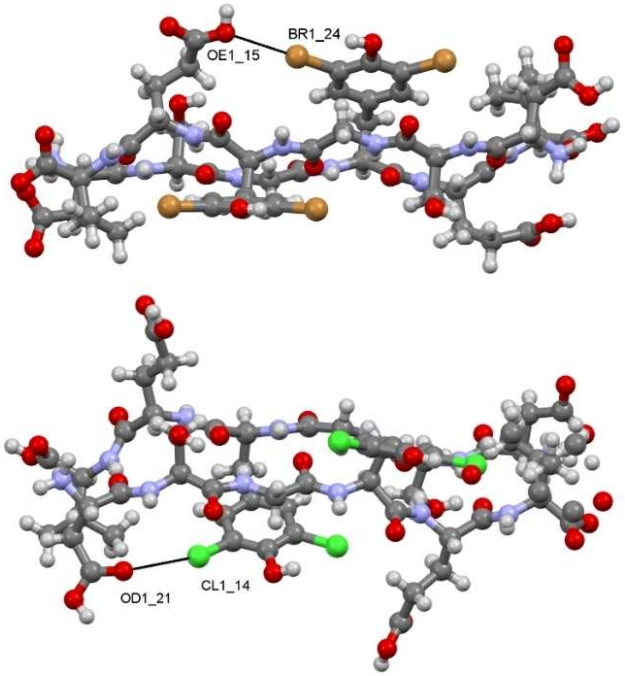

Figure 3. Crystal structure representation of DSGY(3,5-Br)EV (top) and DSGY (3,5-Cl)EV (bottom) where the halogen bonding contacts are shown in black dotted lines. Colour code as in Figure 1 and Hydrogen, white.

reflects the different polarizability of the halogen atoms involved in the HaBs, Br being more polarizable (namely, it has expectedly a more pronounced σ-hole) functions as better HaB donor than Cl, which, in fact, shows a longer and thus weaker HaB.

The presence of the Br···O stabilizing interaction is further confirmed by the Fourier Transform Infrared Spectroscopy (FT–IR) analysis on the crystallized peptide. In fact, the diagnostic band related to the stretching of the carboxylate group of the glutamic acid (E) side chain in DSGY(3,5-Br)EV is redshifted (1415 cm^{-1}) in the brominated peptide (Figure S4) when compared to the wild-type sequence. This suggests a decrease of the electron density over the carboxylate group, which is coherent with its involvement in halogen bonding with the bromine atom.[23] However, similar redshift was not observed in the chlorinated peptide.

Concerning the lateral packing features of the studied sequences, the flanked β-pleated sheets were paired along the *c*-crystallographic axis (Figure S5) by electrostatic interactions involving both C– and N– termini, in addition to the contribution of the charged side chains of aspartate and glutamate residues. Along crystallographic *b*-axis, couples of facing β-sheets running in parallel form the cross-β spine, a peculiar structural motif of amyloid fibrils.

Groups of flanked cross-β structures give rise to higher supramolecular amyloid assemblies, consisting in protofibrils and mature fibrils. In the spine, the facing β-sheets share a common interface that was stabilized by geometrical complementarity between their amino acid side chains (Figure 4). This tightly-interdigitated interface is commonly defined as "steric zipper". Specifically, according to geometrical features based on the intra- and inter-sheet reciprocal orientations,[24] the steric zipper associated to both DSGY(3,5-Br)EV and DSGY(3,5-Cl)EV may be classified as UP-DOWN-FACE=BACK-CLASS 8. The distance between β-sheets forming the zipper – another typical feature of amyloid systems – is 9.81 Å for the brominated sequence (Figure 4b) and 9.45 Å for the chlorinated one (Figure S6).

In addition, antiparallel π···π stacking between the halogenated phenol rings (centroid-centroid distance: 3.59 Å in DSGY (3,5-Br)EV and 3.55 Å in DSGY(3,5-Cl)EV) further contributed to pack adjacent β-sheets along the *b*-crystallographic axis. In DSGY(3,5-Cl)EV, the π···π stacking is also reinforced by dipolar interactions involving the chlorine atoms.

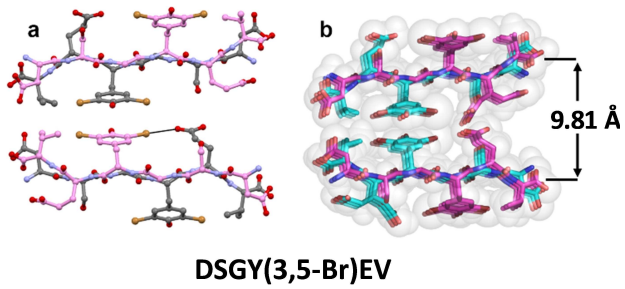

Figure 4. (a) Intrasheet halogen bond occurring between the Br atom and O atom (OE1_15) of the glutamic acid side chain of an adjacent peptide. (b) Steric zipper formed by DSGY(3,5-Br)EV. Interdigitation of facing sheets results in a steric zipper of class 8. The two sheet are separated by 9.81 Å. Colour code is the same reported in Figure 2.

2.2. Non-Covalent Interaction Analysis

It is well-known that cumulative contributes from different non-covalent interactions rule the assembly of proteins/polypeptides and determine their structures.[25] This is true even for a highly flexible sequence such as the one studied here, where, alongside the classical hydrogen bonding network promoting the antiparallel β-sheet arrangement, the presence of various intra- and inter-sheet halogen bonds, π···π interactions, and CH···π interactions influence the stability of the β-sheet, the steric zipper, and the overall crystal packing.

In order to better visualize and understand the role of all of these interactions, we investigated the obtained structures by using Non-Covalent Interaction (NCI) analysis and, in particular, the associated reduced density gradient (RDG) isosurfaces.[26] Specifically, here we have performed DFT calculations with functional M06-2X[27] and standard basis-set 6-311G(d,p) on two sub-packings of the dihalogenated DSGYEV crystals corresponding to two interacting dimers: 1) A dimer of the unit cell containing the β-sheet (Figure 5), and 2) a dimer of the steric zipper (Figure 6). Furthermore, with the aim of evaluating the influence played by the bromine and chlorine atoms on the non-covalent interaction patterns, the corresponding iodinated and hydrogenated systems (which bear iodine and hydrogen atoms at properly optimised positions, respectively) were also taken into account to perform additional reference calculations. The electron densities resulting from all of these computations were afterwards used to perform the above-mentioned NCI analyses. Finally, an estimation of the interaction energies for some relevant intermolecular interactions was also computed.

Looking at the interaction patterns around the halogen atoms in the two peptides, the theoretical studies showed the presence of RDG isosurfaces involving: i) One of the bromine atoms (Br1_24) on the Tyr residue and the oxygen atom (OE1_15) of the Glu residue of an adjacent peptide for DSGY(3,5-Br)EV (Figure 5, top); ii) one chlorine atom (Cl1_14) of the Tyr residue of one peptide chain with one of the oxygen atoms (OD1_21) of the carboxylic group of the Asp residue of a close-by fragment for DSGY(3,5-Cl)EV (Figure 5, bottom). Although the HaB formed by the chlorine atom is weaker than the one involving the Br atom, as suggested by the smaller isosurface associated with the former HaB and proven by the longer halogen bonding distance observed in the X-ray analysis, both the contacts show the distinct directionality features of the classical halogen bonds. In addition, it is worth mentioning that, as observed in the crystal structure of the DSGY(3,5-Br)EV sequence, the bromine atom, which acts as HaB-donor, is also

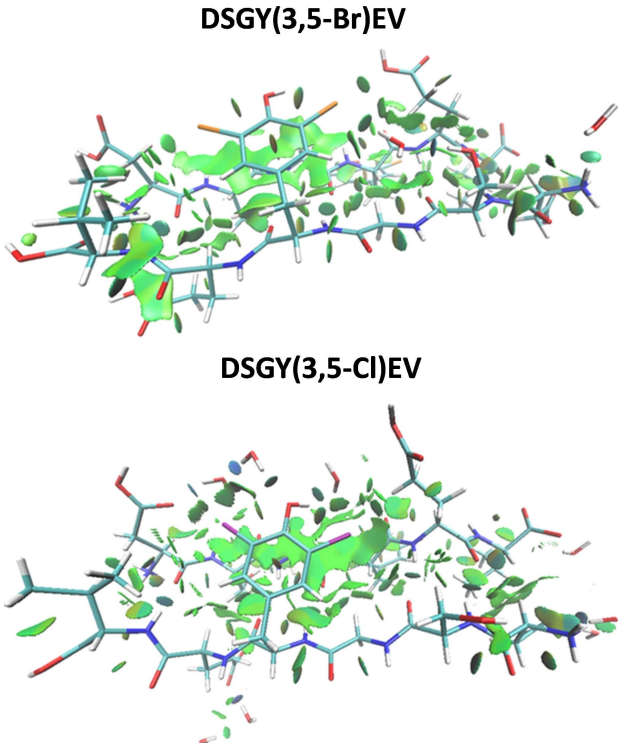

Figure 5. Results of Non-Covalent Interaction (NCI) analyses on dimers of DSGY(3,5-Br)EV (top) and DSGY(3,5-Cl)EV (bottom) where the Reduced Density Gradient (RDG) isosurfaces are shown. NCI analysis highlights the role of π···π interactions and halogen bonds in the halogenated DSGY(3,5-X)EV crystal packing. The halogenated DSGYEV molecules display similar isosurface contacts in the β-sheet. The cut-offs are set at RDG = 0.5 a.u. and -0.05 a.u. $< \mathrm{sign}(\lambda_2)\rho < 0.05$ a.u., while the NCI colour scale is defined according to the values of $\mathrm{sign}(\lambda_2)\rho$, with blue indicating strong attractive interactions, green indicating van der Waals interactions, and red indicating strong non-bonded overlaps.

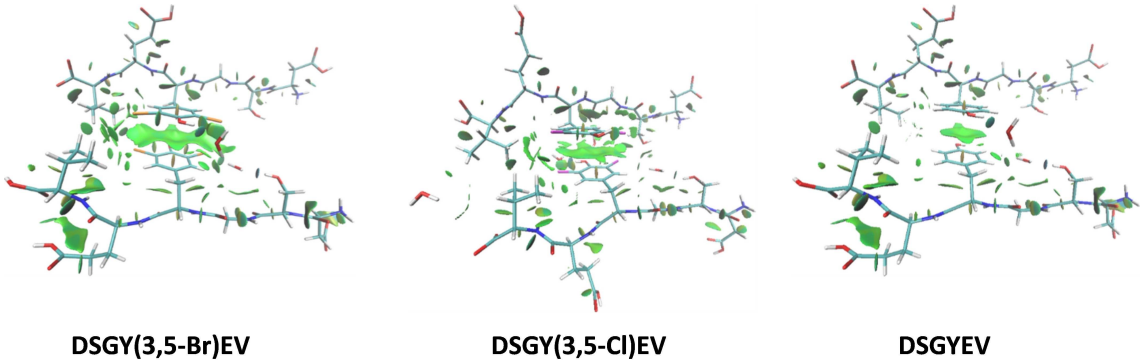

Figure 6. Non-covalent interaction analysis highlights the role of the π···π interactions in the bis-halogenated and hydrogenated DSGY(3,5-X)EV crystal packing. RDG isosurfaces obtained through NCI analyses performed on dimers of DSGY(3,5-Br)EV (left), DSGY(3,5-Cl)EV (centre), and DSGY(3,5-H)EV (right) are shown. DSGY(3,5-H)EV has been obtained substituting the bromine atoms with hydrogen atoms in the original crystallographic brominated structure. See Figure 5 for computational details on the representation of the RDG isosurfaces.

functioning as HB-acceptor towards the hydrogen atom of a water molecule giving rise to the formation of a hydrogen bond, which occurs orthogonally to the Br···O HaB. This contact highlights the amphiphilic character, namely the anisotropic distribution of the electron density, of the bromine atom bound to the Tyr residue atom and underlines, once again, that the formation of HaB and HB, which share one of the interacting sites, takes place with an orthogonal geometry.[22]

As far as the halogen atom polarizability is concerned, further NCI computational studies, which were performed on the systems deriving from the substitution of bromine and chlorine with iodine atoms in their crystal structures, showed more extended RDG isosurfaces around the halogen bonds, while the isosurfaces between the interacting atoms is drastically reduced when Br and Cl atoms are replaced by hydrogen atoms. As expected, these results well correlate with the polarizability scale of the halogen atom series, for which the strength of the halogen bond increases with the deepening of the σ-hole on the halogen atoms, namely with the ability of the halogen atom to function as good HaB-donor (Figure S7 and S8). Overall, the observed Br···O and Cl···O HaBs stabilize the formation of the β-sheet by locking the flexible chains of the Glu residues in DSGY(3,5-Br)EV and of the Asp residues in DSGY (3,5-Cl)EV, respectively.

As highlighted by the structural analysis, the presence of aromatic-aromatic interactions between the halogenated rings also play a key role in the assembly of the modified DSGYEV peptides. In fact, the NCI analysis confirmed the presence of numerous interactions involving the phenyl rings of both simulated systems, showing quite extended RDG isosurfaces around the halogenated aromatic moieties (Figure 6). It is interesting to note that, in both structures, the aromatic units adopt a perfectly parallel face-to-face arrangement of the involved rings but with some differences in the extension of the isosurfaces.

Specifically, in the brominated sequence, the reduced density gradient isosurface associated with the π···π interactions between the rings is much more extended than in the chlorinated system, suggesting that the presence of more polarizable halogen atoms on the phenyl unit could enhance, and thus reinforce, the paring between aromatic rings. This evidence is also supported by the calculations where the halogen atoms were replaced by hydrogen or iodine atoms. In the case of fully hydrogenated rings, the extension of the isosurface is significantly reduced (Figure 6, right panel), while it becomes larger with the iodine atoms (Figures S9 and S10). This set of results clarifies that the presence of the halogen atoms in the sequence not only allows the formation of HaBs that stabilize the β-sheet, but also strengthens π···π stacking interactions among halogenated aromatic rings, thus enhancing the self-assembly capability of the peptides.

2.3. Interaction Energies Estimation

Finally, with the aim of estimating the energies of the halogen bonds and aromatic-aromatic interactions observed in the analyzed systems, we have also decided to reduce the structural complexity, and consequently the computational costs, by considering simpler model systems derived from the crystallographic structures. Specifically, we started from the crystallographic structures (original or with bromine/chlorine atoms properly substituted with iodine or hydrogen atoms) and truncated the side chains of the considered residues at the Cβ atoms. All Cβ atoms were then saturated with hydrogen atoms (Figures S11 and S12). All atoms at the starting positions (namely, those corresponding either to the original crystallographic structures or the crystallographic structures with bromine/chlorine atoms properly substituted with iodine or hydrogen atoms) were then kept fixed (namely, not optimized) to have models as close as possible to the corresponding crystallographic systems. We have, afterwards, performed counterpoise calculations at DFT level, always exploiting functional M06-2X[27] and basis-set 6-311G(d,p).

From the HaB point of view, the calculations showed that all the HaBs were stabilizing interactions and the contact involving bromine and oxygen atoms of the Glu residue was more stable by 3.51 kJ/mol than the HaB involving the chlorine atom, while upon substitution of the bromine atom with iodine atom (in the same geometry of the original brominated crystal structure) the interaction energy is further enhanced by 2.09 kJ/mol. These results, although originated from approximated calculations on model dimers, are in line with those reported in the literature for similar halogen-bonded systems and well mirror the HaB-donor capability of I, Br, and Cl.[28]

Concerning the π···π interactions, as expected from the NCI plots, the interaction energy between brominated aromatic rings in the face-to-face arrangement is stronger than the one between chlorinated rings ($\Delta = 2.73$ kJ/mol), while the substitution of bromine and chlorine atoms with iodine atoms increases the interaction energy for those geometries by almost the same quantity ($\Delta = 2.80$ kJ/mol and $\Delta = 2.70$ kJ/mol, respectively). Differently, the interaction energy decreases significantly when we consider the structures with bromine/chlorine atoms replaced by hydrogen atoms ($\Delta = -26.97$ kJ/mol and $\Delta = -19.91$ kJ/mol, respectively).

Overall, the NCI analysis and the interaction energy calculations confirm that the halogenated tyrosines are involved in an intricate network of halogen-mediated interactions (namely, HaB, π···π and CH···π interactions), which play an important role in stabilizing the β-sheet structures described above, corroborating our data about the enhanced self-assembly of the halogenated DSGYEV peptides.

3. Conclusions

Here we showed that halogenation of Y10 has a deep impact on the supramolecular stabilization of a highly flexible short peptide sequence such as the *N*-term of Aβ. Remarkably, hydrogen-to-halogen substitution on the Y10 promoted the crystallization of the halogenated DSGYEV peptides and allowed the high-resolution analysis of their crystal structures. This unraveled an important role of the halogen atom substitutions

on the stabilization of the steric zipper of the Aβ-spine, also promoting stronger π···π interactions among the aromatic rings of Y10. Computational studies demonstrated the fundamental contribution of the halogen-mediated interactions to providing the overall structural stabilization of the studied sequence. Y halogenation may, thus, develop as a general strategy for stabilizing the structure of otherwise highly polymorphic peptide regions,[29] giving the precise structural information that is essential to facilitate the development of therapeutics.

Experimental Section

Peptide Synthesis and Characterization

Materials

2-CTC resin, *N*-α-Fmoc-L-amino acids and building blocks used during chain assembly were purchased from Iris Biotech GmbH (Marktredwitz, Germany). Ethyl cyanoglyoxylate-2-oxime (Oxyma) was purchased from Novabiochem (Darmstadt, Germany), *N,N′*-dimethylformamide (DMF) and trifluoroacetic acid (TFA) were from Carlo Erba (Rodano, Italy). *N,N′*-diisopropylcarbodiimide (DIC), dichloromethane (DCM), and all other organic reagents and solvents, unless otherwise stated, were purchased in high purity from Sigma-Aldrich (Steinheim, Germany). All solvents for solid-phase peptide synthesis (SPPS) were used without further purification. HPLC grade acetonitrile (ACN) and ultrapure 18.2 Ω water (Millipore-MilliQ) were used for the preparation of all buffers for liquid chromatography. The chromatographic columns were from Phenomenex (Torrance CA, USA). HPLC eluent A: 97.5% H_2O, 2.5% ACN, 0.7%TFA; HPLC eluent B: 30% H_2O, 70% ACN, 0.7% TFA.

Peptide Synthesis: General Procedures

Resin loading

Resin (0.5 mmol/g loading) was swollen in CH_2Cl_2 for 30 min and then washed with DMF (3×3 mL). A solution of entering Fmoc-amino acid and DIEA (1:5) in NMP (3 mL) was added and the resin shaken at r.t. for 4 h. The resin was washed with DMF (2×3 mL) and capping was performed by treatment with methanol/ DIEA in DCM (1×30 min). The resin was then washed with DMF (2×3 mL), CH_2Cl_2 (2×3 mL), and DMF (2×3 mL). The resin was subsequently submitted to fully automated iterative peptide assembly (Fmoc-SPPS).

Peptide Assembly via Iterative Fully Automated Microwave Assisted SPPS

Peptides were assembled by stepwise microwave-assisted Fmoc-SPPS on a Biotage ALSTRA Initiator+ peptide synthesizer, operating in a 0.1 mmol scale. Activation of entering Fmoc-protected amino acids (0.3 M solution in DMF) was performed using 0.5 M Oxyma in DMF/0.5 M DIC in DMF (1:1:1 molar ratio), with a 5 equivalent excess over the initial resin loading. Coupling steps were performed for 20 minutes at 50 °C. Fmoc-deprotection steps were performed by treatment with a 20% piperidine solution in DMF at room temperature (1×10 min). Following each coupling or deprotection step, peptidyl-resin was washed with DMF (4×3.5 mL). Upon complete chain assembly, resin was washed with DCM (5×3.5 mL) and gently dried under a nitrogen flow.

Cleavage from the Resin

Resin-bound peptide was treated with an ice-cold TFA, TIS, water, thioanisole mixture (90:5:2.5:2.5 v/v/v/v, 4 mL). After gently shaking the resin for 2 hours at room temperature, the resin was filtered and washed with neat TFA (2×4 mL). The combined cleavage solutions were worked-up as indicated below.

Work-up and purification

Cleavage mixture was concentrated under nitrogen stream and then added dropwise to ice-cold diethyl ether (40 mL) to precipitate the crude peptide. The crude peptide was collected by centrifugation and washed with further cold diethyl ether to remove scavengers. Residual diethyl ether was removed by a gentle nitrogen flow and the crude peptide was purified by RP-HPLC. Collected peptide was quantified by UV spectroscopy, diluted to 0.05 mM concentration and aliquoted. Peptide aliquots were stored at −80 °C, then lyophilized before use.

RP-HPLC analysis and purification

Analytical RP-HPLC was performed on a Shimadzu Prominence HPLC (Shimadzu) using a Shimadzu Shimpack GWS C18 column (5 micron, 4.6 mm i.d.×150 mm). Analytes were eluted using a binary gradient of mobile phase A (100% water, 0.1% trifluoroacetic acid) and mobile phase B (30% water, 70% acetonitrile, 0.1% trifluoroacetic) using the following chromatographic method: 10% B to 70% B in 14 min; flow rate, 1 ml/min. Preparative RP-HPLC was performed on a Tri Rotar-VI HPLC system (JASCO) using a Phenomenex Jupiter C18 column (10 micron, 21.2 mm i.d.× 250 mm) using the following chromatographic method: 0% B to 90% B in 45 min; flow rate, 14 ml/min. Pure RP-HPLC fractions (> 95%) were combined and lyophilized.

Electro-spray ionization mass spectrometry (ESI-MS)

Electro-spray ionization mass spectrometry (ESI-MS) was performed using a Bruker Esquire 3000+ instrument equipped with an electro-spray ionization source and a quadrupole ion trap detector (Figure S1).

X-Ray Diffraction Analysis - Structural Characterization of DSGY(3,5-Cl)EV and DSGY(3,5-Br)EV Peptides

Data collections were performed at the X-ray diffraction beamline (XRD1) of the Elettra Synchrotron, Trieste (Italy).[30] The crystals were dipped in perfluoropolyether vacuum oil (Fomblin) and mounted on the goniometer head with a nylon loop. Complete datasets were collected at 100 K (nitrogen stream supplied through an Oxford Cryostream 700) through the rotating crystal method. Data were acquired using a monochromatic wavelength of 0.700 Å on a Pilatus 2 M hybrid-pixel area detector. The diffraction data were indexed and integrated using XDS.[31] Scaling have been done using CCP4-Aimless code.[32,33] Crystals appear as very thin needles prone to radiation damage. For the chlorinated peptide we managed to collect a complete dataset from a unique crystal; for the bromine derivative, diffraction decayed even after small doses so two different dataset have to be merged for DSGY(3,5-Br)EV (collected from different crystals randomly oriented).

The structures were solved by the dual space algorithm implemented in the SHELXT code.[34] Fourier analysis and refinement were performed by the full-matrix least-squares methods based on

F^2 implemented in SHELXL-2014.[35] The essential crystal and refinement data are reported in Table S1.

NCI Analysis

Non-Covalent Interaction (NCI) analysis was performed on dimeric systems extracted from the crystal structures of the DSGY(3,5-Br)EV and DSGY(3,5-Cl)EV peptides. Exploiting the Gaussian09 quantum chemistry package,[36] all the calculations have been performed at DFT level using functional M06-2X and the basis-set 6-311G(d,p). These quantum mechanical computations provided us the electron distributions that were afterwards used in the NCI calculations performed by means of the software NCIPLOT-3.0.[26a,b] In particular, in preliminary NCI computations the following options were adopted: a) default cubic grid with a minimum distance of ± 2 Å from the outermost x, y, z coordinates, b) default increment of 0.1 atomic units (a.u.) along the x, y, z directions, c) cutoff interval for the electron density set to [−0.2 a.u., 0.2 a.u.] and d) cutoff for the reduced density-gradient equal to 2.0 a.u.

Estimation of Interaction Energies for Relevant Inter-molecular Interactions

To evaluate the interaction energies (Table S2) associated with relevant contacts between the side chains, we started from the crystallographic structures (original or with bromine/chlorine atoms properly substituted with iodine or hydrogen atoms) and we truncated the side chains of the considered residues at the Cβ atoms. All the Cβ atoms were afterwards saturated with hydrogen atoms (see Figures S11 and 12). For the computation of the interaction energies (Table S2), we have afterwards performed counterpoise calculations at DFT level (M062X functional and 6-311G(d,p) basis-set) keeping fixed (namely, not optimizing) all the atoms at the starting positions (namely, those corresponding to the original crystallographic structures or to the crystallographic structures with bromine/chlorine atoms properly substituted with iodine or hydrogen atoms).

Acknowledgements

The authors are thankful to Fondazione Cariplo for funding the project PHAEDRA, no. 2014-0746.

Conflict of Interest

The authors declare no conflict of interest.

Keywords: halogen bonding · crystal engineering · supramolecular · bromine · peptide

[1] a) M. P. Kummer, M. T. Heneka, *Alzheimer's Res.* **2014**, *6*, 28; b) G. Di Fede, M. Catania, E. Maderna, R. Ghidoni, L. Benussi, E. Tonoli, G. Giaccone, F. Moda, A. Paterlini, I. Campagnani, S. Sorrentino, L. Colombo, A. Kubis, E. Bistafa, B. Ghetti, F. Tagliavini, *Sci. Rep.* **2018**, *8*, 3269.
[2] J. Danielsson, A. Andersson, J. Jarvet, A. Gräslund, *Magn. Reson. Chem.* **2006**, *44*, S114–S121.
[3] R. Riek, D. S. Eisenberg, *Nature* **2016**, *539*, 227–235.
[4] J. A. Hardy, G. A. Higgins, *Science* **1992**, *256*, 184–185.
[5] L. M. Tai, T. Bilousova, L. Jungbauer, S. K. Roeske, K. L. Youmans, C. Yu, W. W. Poon, L. B. Cornwell, C. A. Miller, H. V. Vinters, L. J. Van Eldik, D. W. Fardo, S. Estus, G. Bu, K. H. Gylys, M. J. Ladu, *J. Biol. Chem.* **2013**, *288*, 5914–5926.
[6] F. Hasecke, T. Miti, C. Perez, J. Barton, D. Schölzel, L. Gremer, C. S. R. Grüning, G. Matthews, G. Meisl, T. P. J. Knowles, D. Willbold, P. Neudecker, H. Heise, G. Ullah, W. Hoyer, M. Muschol, *Chem. Sci.* **2018**, *9*, 5937–5948.
[7] a) B. Murray, B. Sharma, G. Belfort, *ACS Chem. Neurosci.* **2017**, *8*, 432–434; b) R. Ahmed, M. Akcan, A. Khondker, M. C. Rheinstädter, J. C. Bozelli, R. M. Epand, V. Huynh, R. G. Wylie, S. Boulton, J. Huang, C. P. Verschoor, G. Melacini, *Chem. Sci.* **2019**, *10*, 6072–6082.
[8] B. Bohrmann, K. Baumann, J. Benz, F. Gerber, W. Huber, F. Knoflach, J. Messer, K. Oroszlan, R. Rauchenberger, W. F. Richter, C. Rothe, M. Urban, M. Bardroff, M. Winter, C. Nordstedt, H. Loetscher, *J. Alzheimer's Dis.* **2012**, *28*, 49–69.
[9] a) M. Nguyen, L. Rechignat, A. Robert, B. Meunier, *ChemistryOpen* **2015**, *4*, 27–31A; b) K. Somavarapu, F. Shen, K. Teilum, J. Zhang, S. Mossin, P. W. Thulstrup, M. J. Bjerrum, M. K. Tiwari, D. Szunyogh, P. M. Søtofte, K. P. Kepp, L. Hemmingsen, *Chem. Eur. J.* **2017**, *23*, 13591–13595.
[10] L. Colombo, A. Gamba, L. Cantù, M. Salmona, F. Tagliavini, V. Rondelli, E. Del Favero, P. Brocca, *Biophys. Chem.* **2017**, *229*, 11–18.
[11] L. Cantù, L. Colombo, T. Stoilova, B. Demé, H. Inouye, R. Booth, V. Rondelli, G. Di Fede, F. Tagliavini, E. Del Favero, D. A. Kirschner, M. Salmona, *Sci. Rep.* **2017**, *7*, 5510.
[12] a) M. P. Kummer, M. Hermes, A. Delekarte, T. Hammerschmidt, S. Kumar, D. Terwel, J. Walter, H.-C. Pape, S. König, S. Roeber, F. Jessen, T. Klockgether, M. Korte, M. T. Heneka, *Neuron* **2011**, *71*, 833–844; b) J. Zhao, J. Wu, Z. Yang, H. Li, Z. Gao, *Chem. Res. Toxicol.* **2017**, *30*, 1085–1092.
[13] M. T. Colvin, R. Silvers, Q. Z. Ni, T. V. Can, I. Sergeyev, M. Rosay, K. J. Donovan, B. Michael, J. Wall, S. Linse, R. G. Griffin, *J. Am. Chem. Soc.* **2016**, *138*, 9663–9674.
[14] A. Piechotta, C. Parthier, M. Kleinschmidt, K. Gnoth, T. Pillot, I. Lues, H.-U. Demuth, S. Schilling, J.-U. Rahfeld, M. T. Stubbs, *J. Biol. Chem.* **2017**, *292*, 12713–12724.
[15] a) R. M. Nisbet, S. D. Nuttall, R. Robert, J. M. Caine, O. Dolezal, M. Hattarki, L. A. Pearce, N. Davydova, C. L. Masters, J. N. Varghese, V. A. Streltsov, *Proteins Struct. Funct. Bioinf.* **2013**, *81*, 1748–1758; b) M. Mukherjee, J. Jana, S. Chatterjee, *ChemistryOpen* **2018**, *7*, 68–79.
[16] A. K. Schütz, T. Vagt, M. Huber, O. Y. Ovchinnikova, R. Cadalbert, J. Wall, P. Güntert, A. Böckmann, R. Glockshuber, B. H. Meier, *Angew. Chem. Int. Ed.* **2015**, *54*, 331–335; *Angew. Chem.* **2015**, *127*, 337–342.
[17] a) L. A. Miles, G. A. N. Crespi, L. Doughty, M. W. Parker, *Sci. Rep.* **2013**, *3*, 1302; b) T. Zhang, L. Nagel-Steger, D. Willbold, *ChemistryOpen* **2019**, *8*, 989–994.
[18] a) A. Bertolani, L. Pirrie, L. Stefan, N. Houbenov, J. S. Haataja, L. Catalano, G. Terraneo, G. Giancane, L. Valli, R. Milani, O. Ikkala, G. Resnati, P. Metrangolo, *Nat. Commun.* **2015**, *6*, 7574; b) M. Erdélyi, *Biochemistry* **2017**, *56*, 2759–2761; c) M. R. Scholfield, M. C. Ford, A.-C. C. Carlsson, H. Butta, R. A. Mehl, P. S. Ho, *Biochemistry* **2017**, *56*, 2794–2802; d) E. Danelius, H. Andersson, P. Jarvoll, K. Lood, J. Gräfenstein, M. Erdélyi, *Biochemistry* **2017**, *56*, 3265–3272.
[19] a) A. Bertolani, A. Pizzi, L. Pirrie, L. Gazzera, G. Morra, M. Meli, G. Colombo, A. Genoni, G. Cavallo, G. Terraneo, P. Metrangolo, *Chem. Eur. J.* **2017**, *23*, 2051–2058; b) A. Pizzi, N. Demitri, G. Terraneo, P. Metrangolo, *CrystEngComm* **2018**, *20*, 5321–5326; c) A. Pizzi, C. Pigliacelli, A. Gori, N. Nonappa, O. Ikkala, N. Demitri, G. Terraneo, V. Castelletto, I. W. Hamley, F. Baldelli Bombelli, P. Metrangolo, *Nanoscale* **2017**, *9*, 9805–9810; d) A. Pizzi, V. Dichiarante, G. Terraneo, P. Metrangolo, *Pept. Sci.* **2018**, *110*, e23088.
[20] J. Zhao, J. Wu, Z. Yang, H. Li, Z. Gao, *Chem. Res. Toxicol.* **2017**, *30*, 1085–1092.
[21] a) G. Cavallo, P. Metrangolo, R. Milani, T. Pilati, A. Priimagi, G. Resnati, G. Terraneo, *Chem. Rev.* **2016**, *116*, 2478–2601; b) G. Bergamaschi, L. Lascialfari, A. Pizzi, M. I. Martinez Espinoza, N. Demitri, A. Milani, A. Gori, P. Metrangolo, *Chem. Commun.* **2018**, *54*, 10718–10721.
[22] a) V. Vasylyeva, S. K. Nayak, G. Terraneo, G. Cavallo, P. Metrangolo, G. Resnati, *CrystEngComm* **2014**, *16*, 8102–8105; b) A. M. S. Riel, R. K. Rowe, E. N. Ho, A.-C. C. Carlsson, A. K. Rappé, O. B. Berryman, P. S. Ho, *Acc. Chem. Res.* **2019**, *52*, 2870–2880.
[23] A. Barth, *Prog. Biophys. Mol. Biol.* **2000**, *74*, 141–173.
[24] J. C. Stroud, *Acta Crystallogr. Sect. D* **2013**, *69*, 540–545.
[25] a) S.-Y. Sheu, D.-Y. Yang, H. L. Selzle, E. W. Schlag, *Proc. Natl. Acad. Sci. USA* **2003**, *100*, 12683–12687; b) P. Auffinger, F. A. Hays, E. Westhof, P. S.

Ho, *Proc. Natl. Acad. Sci. USA* **2004**, *101*, 16789–16794; c) E. Lanzarotti, R. R. Biekofsky, D. A. Estrin, M. A. Marti, A. G. Turjanski, *J. Chem. Inf. Model.* **2011**, *51*, 1623–1633.

[26] a) E. R. Johnson, S. Keinan, P. Mori-Sánchez, J. Contreras-García, A. J. Cohen, W. Yang, *J. Am. Chem. Soc. Rev.C.* **2010**, *132*, 6498–6506; b) J. Contreras-García, E. R. Johnson, S. Keinan, R. Chaudret, J.-P. Piquemal, D. N. Beratan, W. Yang, *J. Chem. Theory Comput.* **2011**, *7*, 625–632; c) D. Arias-Olivares, E. K. Wieduwilt, J. Contreras-García, A. Genoni, *J. Chem. Theory Comput.* **2019**, *15*, 6456–6470.

[27] Y. Zhao, D. G. Thrular, *Theor. Chem. Acc.* **2006**, *120*, 215–241.

[28] a) K. E. Riley, P. Hobza, *Cryst. Growth Des.* **2011**, *11*, 4272–4278; b) K. E. Riley, P. Hobza, *Phys. Chem. Chem. Phys.* **2013**, *15*, 17742–17751; c) A. Gautieri, A. Milani, A. Pizzi, F. Rigoldi, A. Redaelli, P. Metrangolo, *J. Mol. Model.* **2019**, *25*, 124.

[29] J. Pansieri, M. A. Halim, C. Vendrely, M. Dumoulin, F. Legrand, M. Moulin Sallanon, S. Chierici, S. Denti, X. Dagany, P. Dugourd, C. Marquette, R. Antoine, V. Forge, *Chem. Sci.* **2018**, *9*, 2791–2796.

[30] A. Lausi, M. Polentarutti, S. Onesti, J. R. Plaisier, E. Busetto, G. Bais, L. Barba, A. Cassetta, G. Campi, D. Lamba, A. Pifferi, S. C. Mande, D. D. Sarma, S. M. Sharma, G. Paolucci, *Eur. Phys. J. Appl. Phys.* **2015**, *130*, 1–8.

[31] W. Kabsch, *Acta Crystallogr. Sect. D* **2010**, *66*, 125–132.

[32] M. D. Winn, C. C. Ballard, K. D. Cowtan, E. J. Dodson, P. Emsley, P. R. Evans, R. M. Keegan, E. B. Krissinel, A. G. W. Leslie, A. McCoy, S. J. McNicholas, G. N. Murshudov, N. S. Pannu, E. A. Potterton, H. R. Powell, R. J. Read, A. Vagin, K. S. Wilson, *Acta Crystallogr. Sect. D* **2011**, *67*, 235–242.

[33] P. R. Evans, G. N. Murshudov, *Acta Crystallogr. Sect. D* **2013**, *69*, 1204–1214.

[34] G. M. Sheldrick, *Acta Crystallogr. Sect. A* **2015**, *71*, 3–8.

[35] G. M. Sheldrick, *Acta Crystallogr. Sect. C* **2015**, *71*, 3–8.

[36] *Gaussian 09, Revision D. 01, M. J. Frisch, G. W. Trucks, H. B. Schlegel, G. E. Scuseria, M. A. Robb, J. R. Cheeseman, G. Scalmani, V. Barone, B. Mennucci, G. A. Petersson, H. Nakatsuji, M. Caricato, X. Li, H. P. Hratchian, A. F. Izmaylov, J. Bloino, G. Zheng, J. L. Sonnenberg, M. Hada, M. Ehara, K. Toyota, R. Fukuda, J. Hasegawa, M. Ishida, T. Nakajima, Y. Honda, O. Kitao, H. Nakai, T. Vreven, J. A. Montgomery Jr., J. E. Peralta, F. Ogliaro, M. Bearpark, J. J. Heyd, E. Brothers, K. N. Kudin, V. N. Staroverov, R. Kobayashi, J. Normand, K. Raghavachari, A. Rendell, J. C. Burant, S. S. Iyengar, J. Tomasi, M. Cossi, N. Rega, J. M. Millam, M. Klene, J. E. Knox, J. B. Cross, V. Bakken, C. Adamo, J. Jaramillo, R. Gomperts, R. E. Stratmann, O. Yazyev, A. J. Austin, R. Cammi, C. Pomelli, J. W. Ochterski, R. L. Martin, K. Morokuma, V. G. Zakrzewski, G. A. Voth, P. Salvador, J. J. Dannenberg, S. Dapprich, A. D. Daniels, Ö. Farkas, J. B. Foresman, J. V. Ortiz, J. Cioslowski, D. J. Fox, Gaussian, Inc., Wallingford CT* **2009**.

Manuscript received: December 6, 2019
Revised manuscript received: January 7, 2020